SPECT imaging of neuropilin receptor type-1 expression with ^{131}I-labeled monoclonal antibody

XIAOFENG DOU[1,2], JIANGHUA YAN[3], YAFEI ZHANG[1], PENG LIU[1],
YIZHEN JIANG[1], SHA LV[3], FANWEI ZENG[3], XIAOLI CHEN[3], SHENGYU WANG[3],
HAIPENG ZHANG[3], HUA WU[4], HONG ZHANG[2], LIN OUYANG[5] and XINHUI SU[1]

[1]Department of Nuclear Medicine, Zhongshan Hospital Xiamen University, Xiamen, Fujian 361004;
[2]Department of Nuclear Medicine, The Second Affiliated Hospital of Zhejiang University School of Medicine,
Hangzhou, Zhejiang 310052; [3]Cancer Research Center of Medical School, Xiamen University, Xiamen, Fujian 361102;
[4]Department of Nuclear Medicine, The First Affiliated Hospital of Xiamen University, Xiamen, Fujian 361003;
[5]Department of Imaging Medicine, Affiliated Southeast Hospital of Xiamen University, Zhangzhou, Fujian 363000, P.R. China

Abstract. As a novel co-receptor for vascular endothelial growth factor (VEGF), neuropilin receptor type-1 (NRP-1) is overexpressed in several cancers and metastases, and serves as an attractive target for cancer molecular imaging and therapy. Previous single photon emission computerized tomography (SPECT) studies demonstrated that the small NRP-1-targeting peptides ^{99m}Tc-MA-ATWLPPR and ^{99m}Tc-CK3 showed poor tumor imaging quality, because of their rapid blood clearance and very low tumor uptake. Compared with small peptides, monoclonal antibodies (mAbs) can improve imaging of NRP-1-expression, due to their high affinity, specificity and slow extraction. A6-11-26 is a novel monoclonal antibody against NRP-1 b1b2 domain that exhibits inhibition of tumor growth in NPR-1-expressing preclinical models. The aim of the present study was to develop the ^{131}I-labeled anti-NRP-1 monoclonal antibody A6-11-26 as a SPECT probe for imaging of NRP-1-positive tumor. An anti-NRP-1 monoclonal antibody (A6-11-26) was produced by hybridomas and was labeled with iodine-131 by the iodogen method. *In vitro*, the radiolabeling efficiency, radiochemical purity, immunoreactive fraction and stability were assessed. Binding affinity and specificity of ^{131}I-A6-11-26 to NRP-1 were evaluated using human glioblastoma U87MG cells. *In vivo*, biodistribution and SPECT/CT studies were conducted on mice bearing U87MG xenografts after the injection of ^{131}I-A6-11-26 with or without co-injection of unlabeled A6-11-26 antibody. A6-11-26 was generated successfully by hybridoma with high purity (>95%) and was labeled with iodine-131 within 60 min with high labelling efficiency (95.46±3.34%), radiochemical purity (98.23±1.41%). ^{131}I-A6-11-26 retained its immunoreactivity and also displayed excellent stability in mouse serum and PBS solution during 1 to 96 h. Cell uptake assays showed high NRP-1-specific uptake (15.80±1.30% applied activity at 6 h) in U87MG cells. ^{131}I-A6-11-26 bound to NRP-1 with low nanomolar affinity (K_D=1.67±0.14 nM) in U87MG cells. *In vivo*, biodistribution study demonstrated targeting of U87MG glioma xenografts was NRP-1 specific. The tumor uptake was 6.00±1.24%ID/g at 24 h, and the tumor to muscle ratio was 3.20±0.30 at 24 h, and reached the highest level of 6.13±0.24 at 120 h after injection. SPECT imaging studies revealed that ^{131}I-A6-11-26 could clearly identify U87MG tumors with good contrast, especially at 72-120 h after injection. The present study demonstrates that ^{131}I-A6-11-26 is capable of detecting lesions in an NRP-1-expressing tumor with high target selectivity, and may offer a promising SPECT agent for NRP-1 expression positive tumor and encourage further investigation.

Correspondence to: Professor Xinhui Su, Department of Nuclear Medicine, Zhongshan Hospital Xiamen University, 201 Hubin South Road, Xiamen, Fujian 361004, P.R. China
E-mail: suxinhuii@163.com

Professor Lin Ouyang, Department of Imaging Medicine, Affiliated Southeast Hospital of Xiamen University, 269 Zhanghua Road, Zhangzhou, Fujian 363000, P.R. China
E-mail: ddcqzg@126.com

Introduction

Angiogenesis is a critical hallmark of malignancy and is one of the features used frequently by pathologists to make this histological diagnosis and to assess tumor grade (1). Although modulated by various proangiogenic factors, including matrix metalloproteases (MMPS), platelet derived growth factor-β (PDGF-β), tumor necrosis factor-α (TNF-α), and transforming growth factor-β (TGF-β), angiogenesis is principally driven by interactions between vascular endothelial growth factors (VEGFs) and VEGF receptors (VEGFRs), with persistent upregulation of this process being an important factor in the pathology of cancer growth and metastasis (2,3). Of seven VEGF family ligands, such as VEGF-A (VEGF), VEGF-B,

VEGF-C, VEGF-D, VEGF-E, placental growth factor (PlGF) and VEGF-F, VEGF-A is known to be the essential regulator of tumor angiogenesis and endothelial proliferation permeability and survival (4-6). VEGF binds primarily to two tyrosine kinase receptors with high affinity, VEGFR-1 and VEGFR-2 (7). Emerging data suggest that another non-tyrosine kinase receptor identified neuropilins are believed to function as co-receptors for VEGFR-1 and VEGFR-2 (8,9), which trigger the full spectrum of VEGF-induced biological modifications, including proliferation, migration, vascular endothelial cell differentiation and angiogenesis (10,11).

Neuropilins (NRPs) are transmembrane glycoprotein receptors that play an important role in the development of the neuronal and vascular systems as receptors for members of the class-3 semaphorin family (SEMAs) of axonal guidance factors and also for members of the vascular endothelial growth factor (VEGF) family of angiogenesis factors (12,13). In higher eukaryotes, two neuropilin genes, neuropilin-1 (NRP-1) and neuropilin-2 (NRP-2), have been identified. They have approximately 44% amino acid sequence identity and share many structural and biological properties (13-15). Both NRP-1 and NRP-2 contain a large extracellular region and a short cytoplasmic tail of approximately 40 amino acids, lacking any enzymatic activity. Their extracellular region contains three domains: two CUB homology domains (a1a2) as SEMA 3 ligand-binding domain, two coagulation factor V/VIII homology domains (b1b2) as VEGF binding domain, and a MAM domain (c) involved in NRP-1 dimerization (16,17). The binding site for VEGF ligands has been localized to the b1b2 domains of NRP-1 and NRP-2, whereas the binding of semaphorins requires both the a1a2 and b1b2 repeats (18). NRP-1 and NRP-2 interact selectively with different members of the VEGF and semaphorin families and have non-overlapping expression patterns (18). NRP-1 binds VEGF-A165, VEGF-B, VEGF-E, PlGF, SEMA3A, SEMA3B and SEMA3C, whereas NRP-2 binds VEGF-A165,VEGF-A145, VEGF-C, VEGF-D, SEMA3B, SEMA3C and SEMA3F (18,19). However, VEGF-A165 binds 50-fold more strongly to NRP-1 than NRP-2 (20). NRP-1 was found to interact with VEGF-A165 (and other VEGFs), and to act as a VEGF co-receptor that specifically enhances VEGFR-2 signaling to promote VEGF biological activity, including endothelial cell migration, sprouting and angiogenesis (21,22). Transgenic overexpression or knockout of the NRP-1 gene results in lethal abnormalities in the cardiovascular system, suggesting that NRP-1 plays an important role in vasculogenesis and angiogenesis (23). Nevertheless, NRP-2 has different (but overlapping) binding preferences for VEGF family members, and is a co-receptor for VEGFR-3 that is involved in lymphatic endothelial cell function (24).

NRPs are differentially expressed, with NRP-1 detected primarily in arterial endothelial cells, whereas NRP-2 expression is found in venous and lymphatic endothelium (25). Recently, both NRP-1 and NRP-2 are reported to be upregulated in several human tumors, with NRP-1 more preferentially upregulated than NRP-2, and therefore, each is implicated in different aspects of tumor pathogenesis (15,26). For example, blocking NRP-1 function with anti-NRP-1 antibodies inhibited tumor growth (27), whereas anti-NRP-2 antibodies did not affect primary tumor growth, instead they reduced tumor metastasis to sentinel lymph nodes and distant organs (28).

Furthermore, overexpression of NRP-1 is closely correlated with the infiltration and migration of tumors, therapy resistance and poor prognosis (29-32). These findings revealed that NRP-1 might serve as a novel target for cancer diagnosis and therapy. NRP-1 inhibition using monoclonal antibody is considered as a promising strategy for cancer therapy (33,34).

In vivo imaging of tumor-receptor offers a more accurate and real-time assay of receptor expression both for patient stratification and monitoring expression-level changes in response to therapy, without such biopsy-associated pitfalls and the need of repetitive invasive biopsies (35). A variety of small molecular peptides based upon NRP-1 have been labeled with radionuclide ^{99m}T for single photon emission computed tomography (SPECT) molecular imaging of NRP-1 expression (36,37). But, for the small molecules, the probes generally show rapid blood clearance, very low tumor uptake; thus, the imaging quality is poor. Compared with small peptides, monoclonal antibodies (mAbs) can improve imaging of NRP-1-expression, due to their high affinity, specificity and slow extraction. Our previous studies has shown that a novel monoclonal antibody against NRP-1 b1b2 domain (A6-11-26), generated by our laboratory (38), can inhibit tumor proliferation, growth and migration, such as gliomas and breast cancer (39,40), suggesting that A6-11-26 may be an effective agent for NRP-1-targeted imaging and therapy. A6-11-26 specifically binds to NRP-1 b1b2 domain, but not NRP-2 b1b2 domain (data not published), consistent with previous reports (26,27). Therefore, A6-11-26 might be valuable to specifically exploit NRP-1 expression, eliminating any possible undesirable effects mediated by NRP-2. In the present study, we aimed to perform the Iodogen strategy to label the anti-NRP-1 monoclonal antibody A6-11-26 with iodine-131, and further determine whether the resulting SPECT (single-photon emission computed tomography) probe ^{131}I-A6-11-26 is a suitable agent for imaging mice bearing NRP-1 expression glioma U87MG tumors.

Materials and methods

General. Goat anti-mouse IgG antibody was purchased from Santa Cruz Biotechnology (Santa Cruz, CA, USA). Iodogen-coated tubes were purchased from Pierce Biotechnology Ltd. (Rockford, IL, USA). Na^{131}I was obtained from the China Institute of Atomic Energy (Beijing, China). A PD-10 Sephadex G-25 column from GE Healthcare Biosciences, Ltd. (Diegem, Belgium). rProtein A Sepharose columns were purchased from GE Healthcare Bio-Sciences Ltd. (Uppsala, Sweden). DMF-96 gamma counter from Hefei Zhongcheng Electromechanical Technology Development, Co., Ltd. (Hefei, China). CRC-25R dose calibrator from Capintec, Inc. (Ramsey, NJ, USA). BrightView XCT SPECT/CT from Philips Medical Systems, Inc. (Milpitas, CA, USA). Glioma U87 MG cell line was obtained from the Cell Culture Center of Institute of Basic Medical Sciences of Chinese Academy of Medical Sciences (Beijing, China). Female nude mice, 6 and 8 weeks of age, and Balb/c mice were purchased from the Experimental Animal Center of Xiamen University (Xiamen, China).

Production and purification of anti-NRP-1 monoclonal antibodies. An anti-NRP-1 monoclonal antibody (A6-11-26) was

produced by hybridomas derived from mice immunized with a recombinant human NRP-1 b1b2 in our laboratory according to a method previously described (38,40). Briefly, 6-week-old Balb/c mice were injected with hybridoma cells ($2x10^5$-10^6). Seven to 10 days later, ascites (5-10 ml/mouse) with anti-NRP-1 b1b2 monoclonal antibodies (A6-11-26) were centrifuged at 12,000 x g for 5 min and the supernatant were collected. A6-11-26 were purified by rProtein A Sepharose column chromatography as previously described (38), and diluted in PBS. The purity and concentration of A6-11-26 were assessed by 8% SDS-PAGE gel and Bradford assay, respectively.

Titer analysis of A6-11-26. Titer analysis of A6-11-26 was performed by indirect ELISA according to the previously described methods (38). Briefly, 96-well plates were coated with 10 μg/ml of NRP-1 b1b2 in carbonate buffer (pH 9.6) and incubated overnight at 4˚C. Non-specific binding was blocked with 5% non-fat dry milk in PBS (pH 7.5) for 2 h at 37˚C followed by washing three times with washing buffer (0.05% Tween-20 in PBS). The plates were then incubated with supernatant of hybridoma cell (ascites) or A6-11-26 or antiserum IgG of mice for 2 h at 37˚C, respectively. After washing, the plates were incubated with goat anti-mouse IgG-HRP conjugate for 1 h at 37˚C. Finally, the plates were washed as before and o-Phenylenediamine (OPD) was added to develop color. The optical density (OD) was determined at 450 nm by a microplate ELISA reader (Bio-Rad Laboratories, Tokyo, Japan) after the reaction was stopped with 2 M H_2SO_4.

Cellular immunofluorescence staining. Cellular immunofluorescence staining was performed as previously described (29). Briefly, the cell-seeded coverslips were washed and fixed. The diluted (1:100) A6-11-26 and the diluted (1:50) fluorescence (TRITC)-labeled secondary antibody were added. After the U87MG cells were fluorescence-labeled, the fluorescence-labeled secondary antibody was discarded, eluted and stained with Hoechst 33258 staining solution, then observed under a confocal scanning microscope, in which, the excitation wavelength for Hoechst 33258 was ~350 nm and the emission wavelength was ~460 nm; while the maximum absorption wavelength of light for TRITC was 550 nm and the maximum emission wavelength was 620 nm. The relevant images were shot.

Labeling anti-NRP-1 monoclonal antibody A6-11-26 with iodine-131. An anti-NRP-1 monoclonal antibody A6-11-26 was labeled with Na^{131}I by the Iodogen method according to the previous study (41). Briefly, 100 μl 0.01 M phosphate-buffered saline (PBS, pH 7.4) and 22.8 MBq Na^{131}I were added into the prepared Iodogen-coated tubes, and then 20 μg of A6-11-26 was added. Subsequently, the mixture was incubated at room temperature for 15 min with occasional shaking. The reaction was quenched by incubation with 150 μl 0.01 M PBS for 15 min at room temperature. Radiolabeled antibodies were then purified by size-exclusion chromatography using a PD-10 Sephadex G-25 column. For routine quality control of labeling, the labeling efficiency and radiochemical purity of radiolabeled A6-11-26 probes were calculated by paper chromatography on Xinhua filter paper (Hangzhou Xinhua

Paper Industry, Co., Ltd., Hangzhou, China) with the mixture developed with n-butanol:ethanol:ammonia (5:1:2) as the mobile phase. Retention factors (Rf) were: ^{131}I-A6-11-26=0.01, free ^{131}I=0.9-1.0.

Immunoreactive fraction assay. Immunoreactive fraction of ^{131}I-A6-11-26 was performed according to the previously described methods with slight modifications (42,43). Briefly, U87MG cells were washed three times with 0.01 M PBS (pH 7.4) and suspended in a cold PBS with 1% bovine serum albumin (BSA) solution. ^{131}I-A6-11-26 at a constant concentration of 50 ng/ml, in PBS with 1% BSA solution was added to different amounts of cells (final concentration ranging from $2.6x0^6$ to $0.08x10^6$ cells/ml). Cells were incubated for 2 h at 4˚C and then washed twice with 500 μl of cold PBS with 1% BSA solution, before counting cell-associated radioactivity in a gamma counter. The data were plotted as a double inverse plot of the applied radiolabelled antibody over the specific binding as a function of the inverse cell concentration. In this plot, the origin of the abscissa represents infinite cell concentration, i.e., conditions of infinite antigen excess.

In vitro stability analysis. *In vitro* stability in serum or saline was determined by paper chromatography method using strips on Xinhua filter paper (1 cm width and 13 cm length) as described with minor modifications (44,45). Briefly, ^{131}I-A6-11-26 (4.44 MBq) in 250 μl of PBS was added to 2.0 ml of mouse serum or 0.01 M PBS (pH 7.4) and was incubated at 37˚C for 1, 6, 24, 48, 72 and 96 h. At each time-point, the mixture was centrifuged at 16,000 x g for 2 min. A total of 2 μl of the supernatant was placed 2 cm above the lower edge and was allowed to evaporate spontaneously, one strip was developed with the mixture with n-butanol:ethanol:ammonia (5:1:2). After complete development, the paper sheet was removed, dried, and cut into strips of 1 cm width; and then each strip was counted in a gamma counter.

Cell assays. Cell uptake, receptor saturation and internalization assays were performed as previously described with minor modifications (44,46-48). Briefly, the U87MG cell lines were cultured in DMEM supplemented with 10% FBS and 1% penicillin-streptomycin. The cells were maintained in a humidified atmosphere of 5% CO_2 at 37˚C, with the medium changed every two days. A 70-80% confluent monolayer was detached by 0.1% trypsin and dissociated into a single cell suspension for further cell culture.

Cell uptake assays. The U87MG cells were washed three times with 0.01 M PBS (pH 7.4) and dissociated with 0.25% trypsin-EDTA. DMEM medium was then added to neutralize trypsin-EDTA. Cells were spun down and re-suspended with serum-free DMEM. Cells ($0.5x10^6$) were incubated at 37˚C for 0.25 to 2 h with $5.4x10^{-3}$ MBq, 0.02 μg 100 μl ^{131}I-A6-11-26 in 0.5 ml serum-free DMEM medium. The non-specific binding of the probes with U87MG cells was determined by co-incubation with 2.0 μg unlabeled A6-11-26. The cells were washed three times with 0.01 M PBS (pH 7.4) at room temperature. The cells were then washed three times with chilled PBS and spun down at a speed of 7,000-8,000 rpm. The cell pellets at the bottom of the tube were spliced, and the radioactivity of

the pellets was measured using a gamma counter. The uptake (counts/min) was normalized to the percentage of binding for analysis using Excel (Microsoft Software, Inc., Redmond, WA, USA). All experiments were performed in duplicate.

Receptor saturation assay. The U87MG cells ($0.5x10^6$) were plated on 6-well plates one day before the experiment. Cells were washed with PBS three times. Serum-free DMEM (1 ml) was added to each well, followed by the addition of ^{131}I-A6-11-26 ($11.1-599.4x10^{-3}$ MBq, 2-120 nM final concentration). The non-specific binding of ^{131}I-A6-11-26 with U87MG cells was determined by co-incubation with 100 times excess (0.6 μM) of A6-11-26. The plates were then put on ice for 2 h, and the cells were washed with cold PBS three times and detached with TrypLE Express. The radioactivity of the cells was measured using a gamma counter. Specific binding (SB) = total binding (TB) - non-specific binding (NSB). The data were analyzed using GraphPad Prism (GraphPad Software, Inc., San Diego, CA, USA), and the dissociation constant (K_D value) of ^{131}I-A6 was calculated from a 1-site-fit binding curve. All experiments were performed in duplicate.

Internalization assay. The U87MG cells ($0.6x10^6$) were plated on 6-well plates and incubated overnight with internalization buffer (DMEM containing 1% fetal bovine serum) to obtain good cell adherence. The following day, the cells were pretreated with the internalization medium for 1 h at 37˚C. ^{131}I-A6-11-26 ($5.4x10^{-3}$ MBq, 0.02 μg, 100 μl) was added to the medium, and the cells were incubated for 1, 2, 4, 8, 16 and 24 h at 37˚C and 5% CO_2. A 100-fold excess of unlabeled A6-11-26 (2.0 μg) was used to determine non-specific internalization. At each time-point, the internalization was stopped by removal of the medium followed by washing the cells with ice-cold 0.01 M PBS (pH 7.4). Cells were then treated for 5 min (three times) with ice-cold glycine buffer (0.05 mol/l glycine solution, and pH was adjusted to 2.8 with 1 mol/l HCl) to distinguish between cell surface-bound (acid-releasable) and internalized (acid-resistant) radiolabeled antibody. Finally, cells were detached from the plates by incubation with 1.0 M NaOH for 10 min at 37˚C. The medium, the receptor-bound and the internalized fraction of ^{131}I-A6-11-26 were measured in a gamma counter, and the internalized radioactivity rate was calculated and normalized to $1x10^6$ cells/well. All experiments were performed in duplicate.

Biodistribution study. The animal procedures were performed according to a protocol approved by the Institutional Animal Care and Use Committee of Zhongshan Hospital Xiamen University. Approximately $5x10^6$ cultured U87MG cells suspended in PBS were implanted subcutaneously in the right upper shoulders of nude mice. Tumors were allowed to grow to ~0.8-1.0 cm in diameter (25-30 days) and then the tumor-bearing mice were subject to *in vivo* biodistribution and imaging studies.

For biodistribution studies, U87MG tumor-bearing mice (n=5 for each group) were injected with ^{131}I-A6-11-26 (1.2 MBq, 200 μl) through the tail vein. At 24, 48, 72, 96 and 120 h after injection, the mice were sacrificed, and tumors and normal tissues of interest were removed and weighed, and their radioactivity was measured in a gamma counter.

The radioactivity uptake in the tumor and normal tissues was expressed as a percentage of the injected radioactivity per gram of tissue (%ID/g). In order to study the *in vivo* NRP-1 targeting specificity of ^{131}I-A6-11-26, based on the previous studies (44,49), unlabeled A6-11-26 antibody (700 μg) was co-injected with ^{131}I-A6-11-26 in nude mice bearing U87MG tumors (n=5 for each group) via a tail vein, and biodistribution studies were conducted at 120 h after injection.

SPECT/CT imaging. SPECT/CT imaging of tumor-bearing mice was performed on a dual-head SPECT/CT scanner. The mice bearing U87MG tumor (n=5 for each group) were injected with ^{131}I-A6-11-26 (3.7 MBq, 200 μl) with or without co-injection of unlabeled A6-11-26 antibody (700 μg) through the tail vein. At 24, 48, 72, 96 and 120 h after injection, the mice were anesthetized with 2% isoflurane and placed on SPECT/CT bed (ventral side down). SPECT images were acquired in 30 projections over 15 min using a double-headed camera with high energy, high-resolution collimators. CT images were acquired in 30 projections with a 1000 msec exposure time using a 45 kVp X-ray source over 5 min. Whole-body radionuclide images were reconstructed using an iterative ordered subset expectation maximization two dimensional algorithm, and these images were fused with CT images using Syntegra software (Philips Medical Systems). Regions of interest (ROIs) were drawn over the tumor and contralateral muscle, and then the ratio of tumor to contralateral muscle (T/NT) were calculated.

Statistical methods. Statistical analysis was performed using Student's two-tailed t-test for unpaired data. A 95% confidence level was chosen to determine the significance between groups, with a $P<0.05$ being indicated as a significant difference.

Results

Characterization of anti-NRP-1 monoclonal antibodies (A6-11-26). Our previous western blot results showed that A6-11-26 was specifically combined with both NRP-1 b1b2 recombinant protein and whole NPR-1 (38), but not NRP-2 b1b2 domain (data not published). To identify the purity of the current A6-11-26 obtained from ascites, the purified A6-11-26 was resolved by 12% SDS-PAGE (Fig. 1A). A6-11-26 purity was determined to be >95%, as detected by Gray analysis of Quantity One 1D-analysis software (GE Healthcare), at a concentration of 4 mg/ml. Moreover, the results also showed that A6-11-26 was IgG1 isotype.

The purified A6-11-26 was then diluted to measure the titers against NRP-1 b1b2 by indirect ELISA. As shown in Fig. 1B, the purified A6-11-26 can bind to synthetic immunogenic peptides with a titer of $1.28x10^5$.

Immunofluorescence analysis was performed to detected the U87MG cellular expression of NRP-1. As shown in Fig. 2, A6-11-26 could bind well with NRP-1 receptor on the surface of the U87MG cells. Thus, it could be concluded that NRP-1 was expressed in the U87MG cells.

Radioiodination of anti-NRP-1 monoclonal antibody A6-11-26. ^{131}I-A6-11-26 was successfully radioiodinated. The radiolabeling efficiency, radiochemical purity and specific
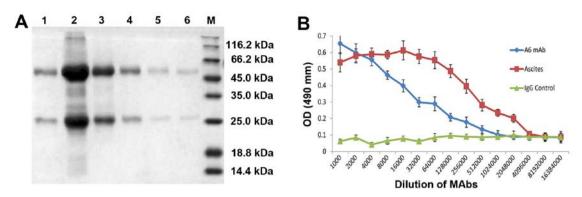
Figure 1. Characterization of anti-NRP-1mAbs (A6-11-26). (A) SDS-PAGE analysis of A6-11-26. M, protein marker; lane 1, IgG1; lane 2, ascites of anti-NRP-1 mAb; lanes 3 to 6, purified A6-11-26. (B) Titer analysis of A6-11-26.
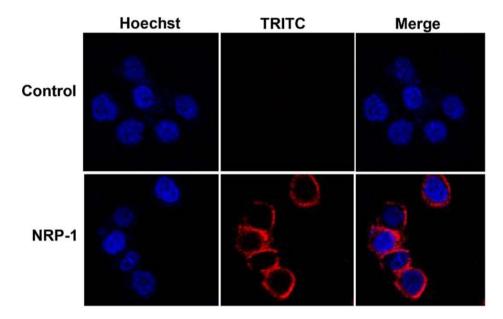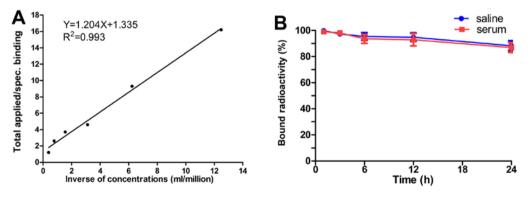

Figure 2. The immunofluorescence of U87MG cells.

Figure 3. Immunoreactivity fraction (A) and *in vitro* stability (B) of ^{131}I-A6-11-26.

activity of ^{131}I-A6-11-26 was 95.46±3.34%, 98.23±1.41% and 180.68±21.4 MBq/μg, respectively.

Immunoreactive fraction assay. As shown in Fig. 3A, the data showed a very close linear relationship of total applied/ specific binding as a function of the inverse cell concentration, which is based on the assumption that the total antigen concentration (cell concentration) is a good enough approximation for the free antigen concentration. Fitting of a straight line to the data by means of linear regression analysis allows an easy and precise determination of the intercept value at the ordinate. This value equals 1/immunoreactive fraction; thus, the immunoreactive fraction of ^{131}I-A6-11-26 was 76.42±5.80%.
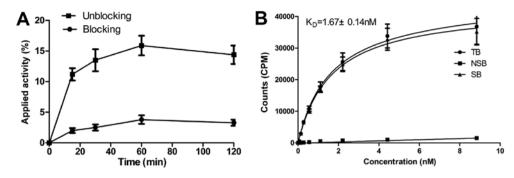
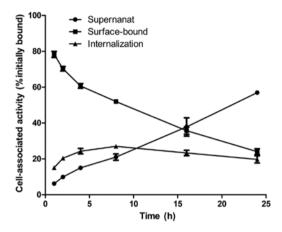Figure 4. Uptake (A) and binding affinity assay (B) of ^{131}I-A6-11-26 in U87MG cells.

Figure 5. Internalization of ^{131}I-A6-11-26 in U87MG cells.

In vitro stability analysis. *In vitro* stability studies showed that >85% of ^{131}I-A6-11-26 remained intact during 1-96 h of incubation in PBS, and declined under 80% in serum at 96 h, indicating that ^{131}I-A6-11-26 maintained more stable in PBS than serum. The stability was not significantly different between in PBS and serum (Fig. 3B).

Cell assays. Cell uptake levels for ^{131}I-A6-11-26 are shown in Fig. 4A. ^{131}I-A6-11-26 quickly accumulated in U87MG cells and reached a highest value of 15.80±1.30% of applied activity at 1 h. When the probe was incubated with large excesses of non-radioactive A6-11-26, its uptake levels in U87MG cells was significantly inhibited (P<0.05) at all incubation time-points.

The binding affinity of ^{131}I-A6-11-26 to NRP-1 was determined through the receptor saturation assay. As shown in Fig. 4B, the K_D value of ^{131}I-A6-11-26 was 1.67±0.14 nM.

The internalization of ^{131}I-A6-11-26 by U87MG cells is presented in Fig. 5. The cell-surface-bound counts gradually decreased, accompanied by a slow increase in counts in the cell culture supernatant. The intracellular trapped radioactivity of ^{131}I-A6-11-26 in U87MG cells gradually increased to a maximum of 27.00±1.00% at 8 h.

Overall, these results strongly suggested that SPECT probe ^{131}I-A6-11-26 had high NRP-1 binding specificity, affinity and low internalization by U87MG cells, which warranted their further evaluation *in vivo*.

Biodistribution study. As shown in Fig. 6 and Table I ^{131}I-A6-11-26 exhibited high accumulation at the tumor

Table I. Comparison of biodistribution for ^{131}I-A6-11-26 in U87MG xenogratfs between 0 µg (unblock) and 700 µg (block).

Organ (%ID/g) (spiked dose)	^{131}I-A6-11-26 (120 h)	
	0 µg (unblock)	700 µg (block)
Tumor	1.60±0.24[a]	0.52±0.11[a]
Heart	0.87±0.23	0.6±0.15
Liver	0.98±0.16	0.87±0.25
Lung	1.70±0.14[a]	0.64±0.07[a]
Spleen	0.75±0.17	0.56±0.14
Kidney	0.74±0.18	0.69±0.21
Brain	0.35±0.05	0.30±0.07
Stomach	0.57±0.13	0.40±0.11
Intestine	0.46±0.10	0.34±0.12
Blood	0.80±0.15	0.61±0.09
Bone	1.24±0.27	0.58±0.10[a]
Muscle	0.27±0.10	0.19±0.08
Pancreas	0.60±0.11	0.42±0.13
Thyroid	2.89±0.58	2.04±0.46
Uptake ratio		
Tumor to blood	1.87±0.50	0.85±0.22
Tumor to muscle	6.13±0.24[a]	2.53±0.86[a]

Data are mean ± SD, expressed as %ID/g. Student's unpaired two-tailed t-test was conducted. [a]P<0.05, comparing 0 µg (unblock) and 700 µg (block) of dose tracer biodistribution at 120 h after injection with ^{131}I-A6-11-26 (n=5 for each group).

bearing U87 MG cells. At 24 h after administration, the tumor uptake was 6.00±1.24%ID/g, significantly higher than that in the other organs except for liver (7.68±1.56%ID/g) and blood (8.00±1.42%ID/g). Moreover, at 48, 72, 96 and 120 h, ^{131}I-A6-11-26 in the tumor still remained at high level, significantly higher than that in the other organs including the liver and blood except thyroid, and in lung and bone had moderate levels. ^{131}I-A6-11-26 provided significantly higher tumor-to-muscle ratios and lower tumor-to-liver and tumor to kidney ratios (Fig. 7A). At 24 h, the ratio of tumor to muscle (T/M=3.20±0.30) was the highest among the tumors to liver (T/L=0.78±0.20), tumor to blood (T/B=0.78±0.10), tumor to
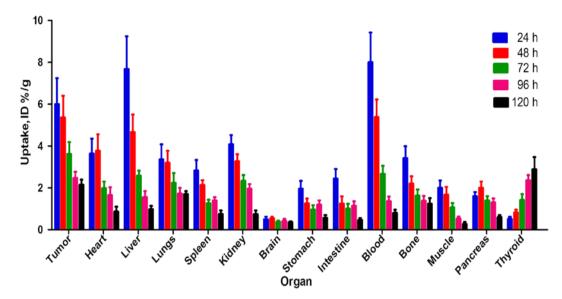
Figure 6. Biodistribution results for ^{131}I-A6-11-26 in U87MG xenogratfs. Data are expressed as %ID/g at various times after intravenous injection of ^{131}I-A6-11-26 (n=5 for each group).
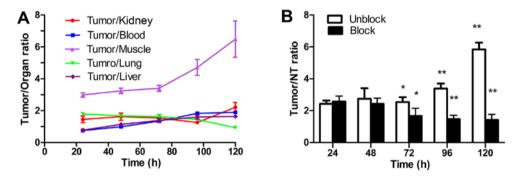

Figure 7. Tumor to normal organ ratios based on biodistribution for ^{131}I-A6-11-26 in U87MG xenogratfs (A) and tumor to contralateral muscle ratios (T/NT) based on SPECT imaging (B). *P<0.05, **P<0.01 comparing of T/NT based on SPECT imaging between 0 µg (unblock) and 700 µg (block) of dose at 120 h after injection with ^{131}I-A6-11-26.
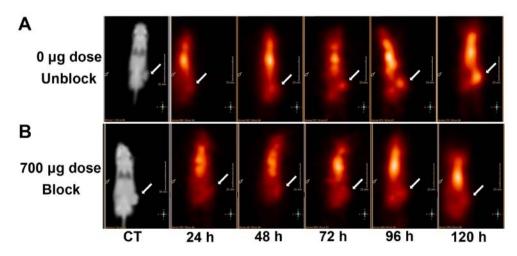

Figure 8. SPET/CT of ^{131}I-A6-11-26 in U87MG xenograft models coinjected with 0 µg dose (A) and 700 µg dose (block, B) of A6-11-26 at 24, 48, 72, 96 and 120 h after injection (n=5 for each group).

kidney (T/K=1.45±0.41), and tumor to lung (T/L=1.79±0.42). Moreover, during 48 to 120 h, the T/M ratio increased gradually over time.

For *in vivo* blocking study (Table I), ^{131}I-A6-11-26 was coinjected with a large excess (700 µg) of the unlabeled A6-11-26 to saturate endogenous and overexpressed NRP-1. The coin-

jection of A6-11-26 significantly reduced the tumor, lung and bone uptake of ^{131}I-A6-11-26 at 120 h after injection (P<0.05), whereas the liver, kidney, blood, spleen and muscle uptake are not significantly changed in the blocking group (P>0.05).

SPECT/CT imaging. SPECT/CT images acquired at 24, 48, 72, 96 and 120 h after injection of ^{131}I-A6-11-26 are shown in Fig. 8A. ^{131}I-A6-11-26 accumulated in the U87MG tumor at 24 h and then showed a gradual increase of uptake. During 72-120 h after injection, U87MG tumors were clearly visible, with good tumor to background contrast. Also observed were high levels of radioactivity accumulation in the kidneys, liver and lungs. However, when coinjected with unlabeled A6-11-26 antibody (700 µg), the tumor was barely visible on SPECT images at 24-120 h after injection (Fig. 8B). Regions of interest (ROIs) analysis of SPECT showed significantly lower ratio of tumor to contralateral muscle (T/NT) for mice injected with 700 µg blocking dose compared to unblocking dose (P<0.05) at 72-120 h post-injection (Fig. 7B).

Discussion

As a co-receptor for vascular endothelial growth factor (VEGF), neuropilin-1 (NRP-1) plays an essential role in the development, progression, invasion of various types of cancers. Inhibition of NRP-1 expression thus appears to be a promising approach for cancer therapy. Several NRP-1 targeting strategies, such as monoclonal antibodies and small-molecule peptides, are being investigated in phases I and Ib clinical trials. Patients with cancer lesions that express NRP-1 may benefit from NRP-1 targeted therapy (33,34). Clinical trials have shown that there is an urgent unmet clinical need for the development of predictive biomarkers permitting patient selection for such therapy. Non-invasive molecular imaging, including SPECT imaging, is an ideal method, since it can offer a more accurate and real-time assay of NRP-1 expression, without such biopsy-associated pitfalls and the need of repetitive invasive biopsies. It has been reported that anti-NRP-1 peptides, such as ATWLPPR and CK3, labeled with radionuclide ^{99m}Tc generally showed rapid blood clearance, but very low tumor uptake and poor tumor imaging quality (36,37). To develop an imaging agent for NRP-1 expression is very important since our goal is to ultimately apply antibody-based SPECT probes for imaging patients.

Due to their highly specific targeting ability, monoclonal antibodies (mAbs) have been considered attractive candidates for targeted therapy and diagnostics in a broad range of medical indications, but especially in oncology. Until now, five technetium-99m (^{99m}Tc) or indium-111 (^{111}In)-labeled mAbs have been approved by the U.S. Food and Drug Administration (FDA) for SPECT diagnostic imaging, among which four are for the imaging of cancer (50). The global sales of mAbs have reached 48 billion dollars in 2011, then in 2015, it is estimated that the sales of antibody drugs only in China are expected to rise spectacularly to 4.6-9.3 billion dollars (51). Hundreds of new mAbs are under development worldwide.

Our previous studies have shown that a novel anti-NRP-1 b1b2 monoclonal antibody A6-11-26, developed by our laboratory, can inhibit tumor proliferation, growth, and migration (39,40), indicating that A6-11-26 may be an effective agent

for NRP-1-targeted imaging and therapy. To further study A6-11-26 imaging performance for targeting NRP-1 herein, we first re-generated monoclonal antibodies A6-11-26 by hybridoma. SDS-PAGE indicated the successful production and purification (>95%) of A6-11-26 sufficient for *in vitro* and *in vivo* cancer research, Furthermore immunofluorescence analysis showed that U87MG cells highly expressed NRP-1, consistent with previous reports (39). Next, A6-11-26 was labeled with ^{131}I using an Iodogen method, and then measured the binding specificity and affinity to NRP-1. The probe ^{131}I-A6-11-26 showed good binding affinity to the U87MG cell NRP-1 with a K_D of 1.67±0.14 nM (Fig. 4B). *In vitro* cell uptake experiments showed that ^{131}I-A6-11-26 had rapid accumulation in the U87MG cells. The uptake reached a plateau in 1 h. This accumulation is NRP-1 specific receptor binding since the rapid cellular uptake of the tracer could be effectively blocked by cold A6-11-26 (Fig. 4A), suggesting that labeling has not influenced the ability of A6-11-26 to bind specifically to NRP-1. These results warranted further evaluation of the probe for *in vivo* NRP-1-targeted tumor imaging.

Our previous study showed that the fluorescence-labeled A6-11-26 could gather at the sites with the transplantation of U87MG tumor cells (39). In the present study, the immuno-reactive fraction assay demonstrated that 76.42±5.80% of the antibodies remain immunoreactive even after the radiolabelling procedure (Fig. 3A). ^{131}I-A6-11-26 mainly localized in U87MG tumors and showed good tumor uptake, retention, and tumor-to-muscle ratios (Figs. 6 and 8). U87MG tumors could be clearly visualized with good contrast by SPECT at 24-120 h after injection, especially at 72-120 h. It is also interesting to find out that the tumor uptake of the ^{131}I-A6-11-26, and tumor to muscle ratio are higher than those of the [^{99m}Tc]Tc-MA-ATWLPPR (36) and ^{99m}Tc-CK3 (37). Evaluation of the probe in mice demonstrated that ^{131}I-A6-11-26 is a promising agent for NRP-1 imaging.

In the present study, the liver, blood and kidney showed high uptake at 24 h after administration. ^{131}I-A6-11-26 was enriched more in the lung, liver and kidney, because of the high natural expression of NRP-1 in the liver (52) and mAbs metabolism through the liver and kidney. The high level of ^{131}I-A6-11-26 in the blood is also possibly due to long circulating mAbs (33,34). Whereas, at 48, 72, 96 and 120 h after injection of ^{131}I-A6-11-26, with ^{131}I-A6-11-26 clearance from blood, the level of the tumor uptake still remained higher than that in the other organs including the liver and blood except thyroid. Moreover, in agreement with previous studies (36,37), radioactivity was found in the lung and bone, since the two normal organs have moderate NRP-1 expression. A high expression of the target in normal organ might appreciable influence the imaging results, especially when the target level in the tumor is low. After optimization of spiking doses, administration to saturate the target expression in normal organ, an increase tumor-normal ratio could be achieved (44,46). Bumbaca *et al* (49) reported that the radiolabelled anti-NRP-1 antibody (MNRP1685A) was co-dosed at 0, 0.1, 0.3, 0.5, 1, 2.5, 5, 7.5, 10, 15 and 25 mg·kg^{-1} unlabelled antibody, at 24 h post dose, a dose-dependent increase in radioactivity was observed in the tumors up to ~2.5-5 mg·kg^{-1}, after which the radioactivity appeared to reach a plateau. The tumor-plasma ratios also increased with dose before reaching a plateau starting with the 2.5 mg·kg^{-1} dose.

Thus, saturation of non-tumor tissue uptake is required in order to achieve tumor uptake (49). In the study, the *in vivo* NRP-1 binding specificity of ^{131}I-A6-11-26 was also verified. When 700 μg of unlabeled A6-11-26 was coinjected, uptakes in high NRP-1 expression organs/tissues, such as the tumor, lung and bone, were both significantly reduced (P<0.05) (Figs. 7B and 8).

However, low tumor accumulation, slow clearance from the circulation, and high energy iodine-131 may hamper its clinical applications. We have currently undertaken studies to improve these parameters. For example, the antibody fragments or anti-NRP-1 affibody molecules and the way of labeling with low energy ^{99m}Tc or ^{111}In could increase rapidly NRP-1 positive tumor targeting ability and gain high imaging contrast within a short period after injection.

Imaging of NRP-1 expression *in vivo* is not only value for treatment optimization of cancer patients, but also may be useful for identifying the sensitivity to chemotherapy in the patients with pancreatic, breast cancer, osteosarcoma, gliomas that are resistant to gemcitabine, 5-fluorouracil (5-FU) or doxorubicin through this mechanism, because NRP-1 over-expression increases constitutive mitogen activated protein kinase (MAPK) signalling through both the ERK and JNK pathways. These pathways appear to promote survival of the pancreatic cancer cell, specifically against anoikis and chemotherapy induced apoptosis (53-55). Furthermore, NRP-1 signaling has been suggested to be involved in development of sorafenib resistance in squamous cell carcinoma of the head and neck (SCCHN) patients (56). Thus, further research for imaging of NRP-1 expression has high clinical translational ability and will likely find broad applications in patient therapy and management for targeting the expression of NRP-1 and cross-talk between MAPK, HER2 and NRP-1 signaling.

In conclusion, an anti-NRP-1 monoclonal antibody A6-11-26 has been easily and successfully radiolabeled with iodine-131. The *in vitro* and *in vivo* study showed the potential of ^{131}I-A6-11-26 as a promising SPECT probe for imaging NRP-1-positive tumor and encouraged further investigation. Nevertheless, since A6-11-26 mAb has a large molecular weight and an immunogenicity that may hinder its application in the clinic, it remains a great challenge to explore a novel small fragment of mAbs or affibody molecules with improved imaging of NRP-1-expression.

Acknowlegements

References

1. Gilbert MR: Renewing interest in targeting angiogenesis in glioblastoma. Lancet Oncol 15: 907-908, 2014.
2. Carmeliet P and Jain RK: Angiogenesis in cancer and other diseases. Nature 407: 249-257, 2000.
3. Spratlin JL, Mulder KE and Mackey JR: Ramucirumab (IMC-1121B): A novel attack on angiogenesis. Future Oncol 6: 1085-1094, 2010.
4. Ferrara N, Gerber HP and LeCouter J: The biology of VEGF and its receptors. Nat Med 9: 669-676, 2003.
5. Inoue M, Hager JH, Ferrara N, Gerber HP and Hanahan D: VEGF-A has a critical, nonredundant role in angiogenic switching and pancreatic beta cell carcinogenesis. Cancer Cell 1: 193-202, 2002.
6. Otrock ZK, Makarem JA and Shamseddine AI: Vascular endothelial growth factor family of ligands and receptors: Review. Blood Cells Mol Dis 38: 258-268, 2007.
7. Cudmore MJ, Hewett PW, Ahmad S, Wang KQ, Cai M, Al-Ani B, Fujisawa T, Ma B, Sissaoui S, Ramma W, et al: The role of heterodimerization between VEGFR-1 and VEGFR-2 in the regulation of endothelial cell homeostasis. Nat Commun 3: 972, 2012.
8. Mac Gabhann F and Popel AS: Interactions of VEGF isoforms with VEGFR-1, VEGFR-2, and neuropilin in vivo: A computational model of human skeletal muscle. Am J Physiol Heart Circ Physiol 292: H459-H474, 2007.
9. Gluzman-Poltorak Z, Cohen T, Herzog Y and Neufeld G: Neuropilin-2 is a receptor for the vascular endothelial growth factor (VEGF) forms VEGF-145 and VEGF-165 [corrected]. J Biol Chem 275: 18040-18045, 2000.
10. Dhakal HP, Naume B, Synnestvedt M, Borgen E, Kaaresen R, Schlichting E, Wiedswang G, Bassarova A, Holm R, Giercksky KE, et al: Expression of vascular endothelial growth factor and vascular endothelial growth factor receptors 1 and 2 in invasive breast carcinoma: Prognostic significance and relationship with markers for aggressiveness. Histopathology 61: 350-364, 2012.
11. Nakayama T, Cho YC, Mine Y, Yoshizaki A, Naito S, Wen CY and Sekine I: Expression of vascular endothelial growth factor and its receptors VEGFR-1 and 2 in gastrointestinal stromal tumors, leiomyomas and schwannomas. World J Gastroenterol 12: 6182-6187, 2006.
12. Staton CA, Kumar I, Reed MW and Brown NJ: Neuropilins in physiological and pathological angiogenesis. J Pathol 212: 237-248, 2007.
13. Bagri A, Tessier-Lavigne M and Watts RJ: Neuropilins in tumor biology. Clin Cancer Res 15: 1860-1864, 2009.
14. Pellet-Many C, Frankel P, Jia H and Zachary I: Neuropilins: Structure, function and role in disease. Biochem J 411: 211-226, 2008.
15. Prud'homme GJ and Glinka Y: Neuropilins are multifunctional coreceptors involved in tumor initiation, growth, metastasis and immunity. Oncotarget 3: 921-939, 2012.
16. Chaudhary B, Khaled YS, Ammori BJ and Elkord E: Neuropilin 1: Function and therapeutic potential in cancer. Cancer Immunol Immunother 63: 81-99, 2014.
17. Plein A, Fantin A and Ruhrberg C: Neuropilin regulation of angiogenesis, arteriogenesis, and vascular permeability. Microcirculation 21: 315-323, 2014.
18. Sulpice E, Plouët J, Bergé M, Allanic D, Tobelem G and Merkulova-Rainon T: Neuropilin-1 and neuropilin-2 act as coreceptors, potentiating proangiogenic activity. Blood 111: 2036-2045, 2008.
19. Geretti E, Shimizu A and Klagsbrun M: Neuropilin structure governs VEGF and semaphorin binding and regulates angiogenesis. Angiogenesis 11: 31-39, 2008.
20. Parker MW, Xu P, Li X and Vander Kooi CW: Structural basis for selective vascular endothelial growth factor-A (VEGF-A) binding to neuropilin-1. J Biol Chem 287: 11082-11089, 2012.
21. Soker S, Takashima S, Miao HQ, Neufeld G and Klagsbrun M: Neuropilin-1 is expressed by endothelial and tumor cells as an isoform-specific receptor for vascular endothelial growth factor. Cell 92: 735-745, 1998.
22. Fuh G, Garcia KC and de Vos AM: The interaction of neuropilin-1 with vascular endothelial growth factor and its receptor flt-1. J Biol Chem 275: 26690-26695, 2000.
23. Kawasaki T, Kitsukawa T, Bekku Y, Matsuda Y, Sanbo M, Yagi T and Fujisawa H: A requirement for neuropilin-1 in embryonic vessel formation. Development 126: 4895-4902, 1999.
24. Kärpänen T, Heckman CA, Keskitalo S, Jeltsch M, Ollila H, Neufeld G, Tamagnone L and Alitalo K: Functional interaction of VEGF-C and VEGF-D with neuropilin receptors. FASEB J 20: 1462-1472, 2006.

25. Herzog Y, Kalcheim C, Kahane N, Reshef R and Neufeld G: Differential expression of neuropilin-1 and neuropilin-2 in arteries and veins. Mech Dev 109: 115-119, 2001.
26. Kim YJ, Bae J, Shin TH, Kang SH, Jeong M, Han Y, Park JH, Kim SK and Kim YS: Immunoglobulin Fc-fused, neuropilin-1-specific peptide shows efficient tumor tissue penetration and inhibits tumor growth via anti-angiogenesis. J Control Release 216: 56-68, 2015.
27. Pan Q, Chanthery Y, Liang WC, Stawicki S, Mak J, Rathore N, Tong RK, Kowalski J, Yee SF, Pacheco G, et al: Blocking neuropilin-1 function has an additive effect with anti-VEGF to inhibit tumor growth. Cancer Cell 11: 53-67, 2007.
28. Caunt M1, Mak J, Liang WC, Stawicki S, Pan Q, Tong RK, Kowalski J, Ho C, Reslan HB, Ross J, et al: Blocking neuropilin-2 function inhibits tumor cell metastasis. Cancer Cell 13: 331-342, 2008.
29. Zhang Y, Liu P, Jiang Y, Dou X, Yan J, Ma C, Fan Q, Wang W, Su F, Tang H, et al: High expression of neuropilin-1 associates with unfavorable clinicopathological features in hepatocellular carcinoma. Pathol Oncol Res 22: 367-375, 2016.
30. Xu Y, Li P, Zhang X, Wang J, Gu D and Wang Y: Prognostic implication of neuropilllin-1 up-regulation in human nasopharyngealc arcinoma. Diagn Pathol 8: 155, 2013.
31. Cheng W, Fu D, Wei ZF, Xu F, Xu XF, Liu YH, Ge JP, Tian F, Han CH, Zhang ZY, et al: NRP-1 expression in bladder cancer and its implications for tumor progression. Tumour Biol 35: 6089-6094, 2014.
32. Zhu H, Cai H, Tang M and Tang J: Neuropilin-1 is overexpressed in osteosarcoma and contributes to tumor progression and poor prognosis. Clin Transl Oncol 16: 732-738, 2014.
33. Weekes CD, Beeram M, Tolcher AW, Papadopoulos KP, Gore L, Hegde P, Xin Y, Yu R, Shih LM, Xiang H, et al: A phase I study of the human monoclonal anti-NRP1 antibody MNRP1685A in patients with advanced solid tumors. Invest New Drugs 32: 653-660, 2014.
34. Patnaik A, LoRusso PM, Messersmith WA, Papadopoulos KP, Gore L, Beeram M, Ramakrishnan V, Kim AH, Beyer JC, Mason Shih L, et al: A Phase Ib study evaluating MNRP1685A, a fully human anti-NRP1 monoclonal antibody, in combination with bevacizumab and paclitaxel in patients with advanced solid tumors. Cancer Chemother Pharmacol 73: 951-960, 2014.
35. Tolmachev V, Stone-Elander S and Orlova A: Current approaches to the use of radiolabeled tyrosine kinase-targeting drugs for patient stratification and treatment response monitoring: Prospects and pitfalls. Lancet Oncol 11: 992-1000, 2010.
36. Perret GY, Starzec A, Hauet N, Vergote J, Le Pecheur M, Vassy R, Léger G, Verbeke KA, Bormans G, Nicolas P, et al: In vitro evaluation and biodistribution of a 99mTc-labeled anti-VEGF peptide targeting neuropilin-1. Nucl Med Biol 31: 575-581, 2004.
37. Feng GK, Liu RB, Zhang MQ, Ye XX, Zhong Q, Xia YF, Li MZ, Wang J, Song EW, Zhang X, et al: SPECT and near-infrared fluorescence imaging of breast cancer with a neuropilin-1-targeting peptide. J Control Release 192: 236-242, 2014.
38. Li X, Luo F, Wang S, Ni E, Tang X, Lv H, Chen X, Chen L and Yan J: Monoclonal antibody against NRP-1 b1b2. Hybridoma (Larchmt) 30: 369-373, 2011.
39. Chen L, Miao W, Tang X, Zhang H, Wang S, Luo F and Yan J: Inhibitory effect of neuropilin-1 monoclonal antibody (NRP-1 MAb) on glioma tumor in mice. J Biomedical Nanotechnol 9: 551-558, 2013.
40. Zeng F, Luo F, Lv S, Zhang H, Cao C, Chen X, Wang S, Li Z, Wang X, Dou X, et al: A monoclonal antibody targeting neuropilin-1 inhibits adhesion of MCF7 breast cancer cells to fibronectin by suppressing the FAK/p130cas signaling pathway. Anticancer Drugs 25: 663-672, 2014.
41. Yang C, Yun Q, Sun H, Yang G, Liang T, Zhang C, Song J, Han J and Hou G: Non-invasive imaging of Toll-like receptor 5 expression using 131I-labeled mAb in the mice bearing H22 tumors. Oncol Lett 7: 1919-1924, 2014.
42. Lindmo T, Boven E, Cuttitta F, Fedorko J and Bunn PA Jr: Determination of the immunoreactive fraction of radiolabeled monoclonal antibodies by linear extrapolation to binding at infinite antigen excess. J Immunol Methods 72: 77-89, 1984.
43. Malviya G1, Anzola KL, Podestà E, Laganà B, Del Mastro C, Dierckx RA, Scopinaro F andSignore A: 99mTc-labeled rituximab for imaging B lymphocyte infiltration in inflammatory autoimmune disease patients. Mol Imaging Biol 14: 637-646, 2012.
44. Su X, Cheng K, Jeon J, Shen B, Venturin GT, Hu X, Rao J, Chin FT, Wu H and Cheng Z: Comparison of two site-specifically 18F-labeled affibodies for PET imaging of EGFR positive tumors. Mol Pharm 11: 3947-3956, 2014.
45. Zhao Q, Yan P, Wang RF, Zhang CL, Li L and Yin L: A novel 99mTc-labeled molecular probe for tumor angiogenesis imaging in hepatoma xenografts model: A pilot study. PLoS One 8: e61043, 2013.
46. Su X, Cheng K, Liu Y, Hu X, Meng S and Cheng Z: PET imaging of insulin-like growth factor type 1 receptor expression with a 64Cu-labeled Affibody molecule. Amino Acids 47: 1409-1419, 2015.
47. Kato Y, Vaidyanathan G, Kaneko MK, Mishima K, Srivastava N, Chandramohan V, Pegram C, Keir ST, Kuan CT, Bigner DD, et al: Evaluation of anti-podoplanin rat monoclonal antibody NZ-1 for targeting malignant gliomas. Nucl Med Biol 37: 785-794, 2010.
48. Wang X, Aldrich MB, Marshall MV and Sevick-Muraca EM: Preclinical characterization and validation of a dual-labeled trastuzumab-based imaging agent for diagnosing breast cancer. Chin J Cancer Res 27: 74-82, 2015.
49. Bumbaca D, Xiang H, Boswell CA, Port RE, Stainton SL, Mundo EE, Ulufatu S, Bagri A, Theil FP, Fielder PJ, et al: Maximizing tumour exposure to anti-neuropilin-1 antibody requires saturation of non-tumour tissue antigenic sinks in mice. Br J Pharmacol 166: 368-377, 2012.
50. van Dongen GA, Visser GW, Lub-de Hooge MN, de Vries EG and Perk LR: Immuno-PET: A navigator in monoclonal antibody development and applications. Oncologist 12: 1379-1389, 2007.
51. Li X, Gong M, Xu W and Tang L: Market dynamics of antibody drugs in both domestic and abroad. Drugs Clin 27: 185-191, 2012.
52. Bergé M, Allanic D, Bonnin P, de Montrion C, Richard J, Suc M, Boivin JF, Contrerès JO, Lockhart BP, Pocard M, et al: Neuropilin-1 is upregulated in hepatocellular carcinoma and contribut- es to tumour growth and vascular remodelling. J Hepatol 55: 866-875, 2011.
53. Han Z, Jiang G, Zhang Y, Xu J, Chen C, Zhang L, Xu Z and Du X: Effects of RNA interference-mediated NRP-1 silencing on the proliferation and apoptosis of breast cancer cells. Mol Med Rep 12: 513-519, 2015.
54. Wey JS, Gray MJ, Fan F, Belcheva A, McCarty MF, Stoeltzing O, Somcio R, Liu W, Evans DB, Klagsbrun M, et al: Overexpression of neuropilin-1 promotes constitutive MAPK signalling and chemoresistance in pancreatic cancer cells. Br J Cancer 93: 233-241, 2005.
55. Yue B, Ma JF, Yao G, Yang MD, Cheng H and Liu GY: Knockdown of neuropilin-1 suppresses invasion, angiogenesis, and increases the chemosensitivity to doxorubicin in osteosarcoma cells: an in vitro study. Eur Rev Med Pharmacol Sci 18: 1735-1741, 2014.
56. Mehta S, Moon J, Hashmi M, Leblanc M, Huang CH, Rinehart E, Wolf GT, Urba SG, Banerjee SK and Williamson S: Predictive factors in patients with advanced and metastatic squamous cell carcinoma of the head and neck: A study based on SWOG protocol S0420. Oncol Rep 29: 2095-2100, 2013.